

# Scalable Algorithms for Power Function Calculations of quantum states in NISQ Era

Wencheng Zhao,<sup>1,\*</sup> Tingting Chen,<sup>1,\*</sup> and Ruyu Yang<sup>2,†</sup>

<sup>1</sup>*China University of Mining and Technology, College of Sciences, Beijing 100083, China*

<sup>2</sup>*Graduate School of China Academy of Engineering Physics, Beijing 100193, China*

(Dated: September 6, 2023)

Quantum computing stands at the vanguard of science, focused on exploiting quantum mechanical phenomena like superposition and entanglement. Its goal is to create innovative computational models that address intricate problems beyond classical computers' capabilities. In the Noisy Intermediate-Scale Quantum (NISQ) era, developing algorithms for nonlinear function calculations on density matrices is of paramount importance. This project endeavors to design scalable algorithms for calculating power functions of mixed quantum states. This study introduces two algorithms based on the Hadamard Test and Gate Set Tomography. Additionally, a comparison of their computational outcomes is offered, accompanied by a meticulous assessment of errors inherent in the Gate Set Tomography-based approach.

## I. INTRODUCTION

In recent years, remarkable strides have been taken in constructing and managing intermediate-scale quantum systems housing hundreds or even thousands of entangled qubits[1–5]. Computing nonlinear functions of density matrices on Noisy Intermediate-Scale Quantum (NISQ) computers is a fundamental yet challenging endeavor[6, 7]. There are many important functions that are nonlinear functions of the density matrix[8], including Renyi entropy[9–11], Von Neumann entropy[12, 13], Quantum Fisher information[14, 15], fidelity of mixed states[16], and distance between density matrices[17]. Their significance spans quantum information, condensed matter physics, and quantum chemistry[18], while also finding application in virtual distillation[19–22] and other domains[23–29].

Prior methodologies for nonlinear transformations relied on simultaneously preparing multiple copies of a quantum state[30] and collective measurements[31]. These approaches necessitated a large number of qubits. For instance, when computing  $Tr\{\rho^m\}$ , with  $\rho$  representing the density matrix defined over  $n$  qubits, these methods required  $nm$  qubits. However, in the NISQ era, the number of qubits is still insufficient, rendering it inadequate to achieve quantum advantage within these algorithms[6]. Conversely, researchers have advocated for constructing the classical shadow of  $\rho$  and subsequently employing it to compute the purity  $Tr\{\rho^2\}$ [32]. While this approach still entails exponential resources relative to the number of qubits, it is perceived as an enhancement over traditional State Tomography[33]. Nevertheless, ongoing exploration of such methods is delimited to purity, which corresponds to quadratic functions of the density matrix. For higher-order functions like  $Tr\{\rho^m\}$ , there is no substantiated indication that these methods sustain an advantage over classical approaches.

To more efficiently exploit quantum computers in the NISQ era, we aim to design algorithms that employ the same number of qubits as  $\rho$  and exhibit polynomial growth in circuit depth with the largest order of nonlinear transformations. A technique for generating mixed states involves initiating from an initial state and applying quantum gates randomly based on a specific probability distribution. The resultant final states post the application of diverse quantum gates to the initial state might not be orthogonal. We ascertain the presence of the algorithm we want, assuming the knowledge about how to construct the intended mixed state by utilizing random circuits.

In this study, we introduce two distinct algorithms, both characterized by their shared utilization of the Grover gate  $G = I - 2|0\rangle\langle 0|$ . The primary aim of both algorithms is to compute the power series expansion  $Tr\{\rho^m\}$  for a nonlinear function in the context of a multi-qubit quantum mixed state  $\rho$ . The first algorithm is based on the Hadamard Test(HT). It involves transforming an auxiliary qubit (usually  $|0\rangle\langle 0|$ ) into a superposition state using the Hadamard gate. After a controlled gate operation, another Hadamard gate extracts essential data, finalizing the calculation. Our algorithm is Hadamard Test-based but introduces an innovative approach: we deploy a quantum pure state circuit to simulate  $Tr\{G^{m-1}\rho\}$  computation for a quantum mixed state, by employing weighted averages across multiple measurements. The second algorithm begins by mathematically converting the calculation of  $Tr\{\rho^m\}$  for the desired quantum state into  $Tr\{G^m\}$ . A comprehensive understanding of  $G^m$  is acquired through Gate Set Tomography(GST)[34, 35] in a subspace, facilitating the calculation and estimation of  $Tr\{G^m\}$  through mathematical processing. Compared to the Hadamard Test-based algorithm, this approach entails fewer qubits and two-qubit gates within the circuit. Moreover, this method introduces a novel result-processing technique rooted in reconstruction. Both algorithms exhibit scalability, with time complexity that doesn't experience exponential growth with the number of qubits.

The structure of this paper is outlined as follows. We

\* These authors contributed equally to the work.

† [yangruyu96@gmail.com](mailto:yangruyu96@gmail.com)

commence by introducing the Hadamard test-based algorithm in Section II. Subsequently, we elucidate the application of the GST method in Section III for extracting pertinent information from the subspace. Section IV is dedicated to error analysis and complexities. In Section V, we present computational results garnered from the preparation of the quantum mixed state  $\rho$  and the subsequent application of both algorithms. Notably, we compare the variations in calculations for the identical quantum state when utilizing the two distinct algorithms. A concise recapitulation of this article is offered in Section VI.

In the appendix, we delve into specific scenarios, enabling the applicability of our algorithms to various instances of solving nonlinear functions within quantum mixed states. Additionally, we conduct result simulations under the presence of noise to elucidate the impact of noise-induced uncertainty on outcomes. Furthermore, we also investigate the dimensions of the subspaces that need to be studied when applying our algorithms to more general functions.

## II. TRACE ESTIMATION OF HADAMARD TEST

### A. Theoretical Part of Hadamard Test

In this section, we show how to calculate  $Tr\{\rho^m\}$  using HT[36–39]. Firstly, we show how the quantum state is encoded in a quantum channel.

Suppose the  $n$ -qubits quantum mixed state is given by  $\rho = \sum_{i=1}^{\alpha} p_i U_i |0\rangle\langle 0|^{\otimes n} U_i^\dagger = \sum_{i=1}^{\alpha} p_i |\psi_i\rangle\langle\psi_i|$ , where  $\alpha$  random unitary gates  $U_i$  and probabilities  $p_i$  are known. Define the  $G$  gate as:  $G = \sum_{j=1}^{\alpha} p_j U_j G_0 U_j^\dagger$ , where  $G_0 = I_{2^n} - 2|0\rangle\langle 0|^{\otimes n}$  is the Grover operator. Then we can express the quantum channel as  $G = I_{2^n} - 2\rho$ , and  $G^k = (I_{2^n} - 2\rho)^k$ . In this way, We encode the state  $\rho$  into a non-unitary quantum channel  $G$ .

Next, we show how HT works. In general, one ancilla qubit is required for HT. The quantum circuit has been shown in Fig 1. The computation process is as follows.

In the region denoted as A, the quantum state of the circuit at this point is given by:

$$|0\rangle\langle 0| \otimes \rho. \quad (1)$$

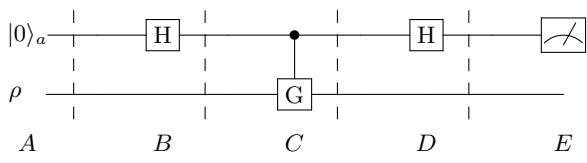


FIG. 1. Illustrative diagram of the Hadamard Test circuit. The diagram features two distinct paths, which have been divided into five segments for ease of computation. The first path encompasses two  $H$  gates and a single measurement gate, while the second path incorporates a *controlled*– $G$  gate.

In the B region, after applying the Hadamard gate, the state of the ancillary qubit is transformed as Eq.(2):

$$H|0\rangle\langle 0|H^\dagger = \frac{1}{2}(|0\rangle\langle 0| + |0\rangle\langle 1| + |1\rangle\langle 0| + |1\rangle\langle 1|). \quad (2)$$

The overall state of the circuit is given by:

$$\frac{1}{2}(|0\rangle\langle 0| + |0\rangle\langle 1| + |1\rangle\langle 0| + |1\rangle\langle 1|) \otimes \rho. \quad (3)$$

Then, the state undergoes the action of the controlled G gate:

$$CG^k = |0\rangle\langle 0| \otimes I + |1\rangle\langle 1| \otimes G^k. \quad (4)$$

Thus, the state in the region C is:

$$\begin{aligned} & \frac{1}{2}(|0\rangle\langle 0| \otimes \rho) + \frac{1}{2}|0\rangle\langle 1| \otimes \rho(G^k)^\dagger + \\ & \frac{1}{2}|1\rangle\langle 0| \otimes G^k \rho + \frac{1}{2}|1\rangle\langle 1| G^k \rho(G^k)^\dagger. \end{aligned} \quad (5)$$

Subsequently, the auxiliary qubit undergoes another Hadamard gate operation. Consequently, the state within the region D is then given by:

$$\begin{aligned} & \frac{1}{2}[(H|0\rangle\langle 0|H^\dagger) \otimes \rho + (H|0\rangle\langle 1|H^\dagger) \otimes \rho(G^k)^\dagger \\ & + (H|1\rangle\langle 0|H^\dagger) \otimes G^k \rho + (H|1\rangle\langle 1|H^\dagger) \otimes G^k \rho(G^k)^\dagger]. \end{aligned} \quad (6)$$

Expanding each term results as:

$$\begin{aligned} & \frac{1}{4}|0\rangle\langle 0| \otimes [\rho + \rho(G^k)^\dagger + (G^k)\rho + (G^k)\rho(G^k)^\dagger], \\ & \frac{1}{4}|0\rangle\langle 1| \otimes [\rho - \rho(G^k)^\dagger + (G^k)\rho - (G^k)\rho(G^k)^\dagger], \\ & \frac{1}{4}|1\rangle\langle 0| \otimes [\rho + \rho(G^k)^\dagger - (G^k)\rho - (G^k)\rho(G^k)^\dagger], \\ & \frac{1}{4}|1\rangle\langle 1| \otimes [\rho - \rho(G^k)^\dagger - (G^k)\rho + (G^k)\rho(G^k)^\dagger], \end{aligned} \quad (7)$$

The expression above can be denoted as follows Eq.(8):

$$\rho' = |0\rangle\langle 0| \otimes a_{11} + |0\rangle\langle 1| \otimes a_{12} + |1\rangle\langle 0| \otimes a_{21} + |1\rangle\langle 1| \otimes a_{22} \quad (8)$$

Under the computational basis measurement in region E, the measurement operators are defined as  $M_0 = |0\rangle\langle 0| \otimes I$  and  $M_1 = |1\rangle\langle 1| \otimes I$ . The probability distribution over the outcomes of the measurement are :

$$\begin{aligned} P(0) &= Tr\{M_0 \rho' M_0^\dagger\} = |a_{11}|^2 \\ &= \frac{1}{2} + \frac{1}{2} Tr\{G^k \rho\}, \end{aligned} \quad (9)$$

$$\begin{aligned} P(1) &= Tr\{M_1 \rho' M_1^\dagger\} = |a_{22}|^2 \\ &= \frac{1}{2} - \frac{1}{2} Tr\{G^k \rho\}. \end{aligned} \quad (10)$$

The expression for  $Tr\{G^k \rho\}$  can be derived, with the ultimate goal of estimating:

$$\begin{aligned} Tr\{\rho^{m+1}\} &= Tr\left\{\left(\frac{1}{2}G - \frac{1}{2}I\right)^m \rho\right\} \\ &= \frac{1}{2^m} \sum_k C_m^k (-1)^{m-k} Tr\{G^k \rho\}. \end{aligned} \quad (11)$$

Let:

$$p_k = \frac{1}{2^m} C_m^k, \quad (12)$$

$$x_k = (-1)^{m-k} Tr\{G^k \rho\}. \quad (13)$$

The above equation can be transformed into an expectation calculation:

$$Tr\{\rho^{m+1}\} = \sum_k p_k x_k = E_k(x_k). \quad (14)$$

To estimate the expectation, we need to generate quantum circuits using a random sampling method. For each circuit, we sample  $m$  times, with a  $\frac{1}{2}$  probability of adding a  $CG$  gate to the circuit and a  $\frac{1}{2}$  probability of doing nothing. After generating multiple circuits, we take the average of the results.

## B. Algorithm Process of Hadamard Test

We summarize the algorithm as follows:

1. Set the initial state to  $|0\rangle^{\otimes n+1}$ .
2. Randomly select  $U_i$  with probability  $p_i$  to act on the target qubits.
3. Apply a Hadamard gate to the ancilla qubit.
4. Sample  $m$  times, with a  $\frac{1}{2}$  probability of adding a  $CG$  gate to the circuit and a  $\frac{1}{2}$  probability of doing nothing.
5. Apply another Hadamard gate to the ancilla qubit.
6. Perform a computational basis measurement on the auxiliary qubit circuit.
7. Repeat the above steps  $N$  times and take the average.

## III. TRACE ESTIMATION OF QUANTUM TOMOGRAPHY

### A. Theoretical Part of Tomography

Quantum tomography denotes a suite of techniques aiming to reconstruct an unknown quantum channel or

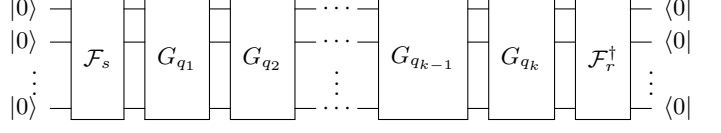


FIG. 2. This is a quantum circuit with  $n$ -Qubits used to compute  $Tr\{\rho_r^\dagger \mathcal{G}_q^k \rho_s \mathcal{G}_q^k\}$ . First, we add the prepared state  $\rho_r^\dagger$  to the circuit. Next, we apply the operator  $\mathcal{G}_q^k$ . Then, we add  $\rho_s$  to the circuit. The circuit will automatically apply the gate  $(\mathcal{G}_q^k)^\dagger$  during the process.

state through experimental measurements. This process is pivotal for the comprehensive understanding and authentication of quantum apparatus [40–44]. Nevertheless, the scalability of quantum tomography poses a challenge, as the indispensable measurements and computational resources experience exponential growth in tandem with qubit numbers. In the context of our current research problem, there is a silver lining: the subspace we are investigating maintains a dimension that remains unaffected by the number of qubits. This distinctive feature becomes particularly advantageous. In the subsequent section, we expound on our utilization of the GST method to adeptly extract the pertinent information from this designated subspace.

In comparison with the preceding context, the process of preparing mixed quantum states adheres to the same approach as the Hadamard Test method. This methodology necessitates the application of an assortment of stochastically selected gates  $\{(U_i)_{2^n \times 2^n}, i = 1, 2, \dots, \alpha\}$  onto the initial quantum state (typically  $|0\rangle\langle 0|^{\otimes n}$ ), resulting in the emergence of a mixed quantum state. The primary objective revolves around the computation of  $Tr\{\rho^m\}$ , which is achieved through the intermediary of  $Tr\{G^m\}$ , where  $G = I - 2\rho$ . We can express  $Tr\{\rho^m\}$  as

$$Tr\{\rho^m\} = \frac{1}{2^m} \sum_k C_m^k (-1)^{m-k} Tr\{G^k\}. \quad (15)$$

Similar to the approach employed in the HT-based algorithm, we can estimate this summation by leveraging the Monte Carlo method. This involves conducting multiple circuit samplings in accordance with their respective probabilities and subsequently calculating the average. Through this process, we can attain the sought-after value of  $Tr\{\rho^m\}$ . The circuit responsible for this estimation is depicted in Fig 2.

### 1. Mathematical Treatment:

We start with the unitary quantum gate  $G_0$ :

$$(G_0)_{2^n \times 2^n} = I_{2^n} - 2|0\rangle\langle 0|^{\otimes n} = \begin{pmatrix} -1 & 0 & \dots & 0 \\ 0 & 1 & \dots & 0 \\ \vdots & \vdots & \ddots & \vdots \\ 0 & 0 & \dots & 1 \end{pmatrix}. \quad (16)$$

Through the application of random unitary gates  $U_i$  to the initial gate  $G_0$ , a set of  $\alpha$  distinct gates is generated. These gates are denoted as  $G_i = U_i G_0 U_i^\dagger$ . The composite gate  $G$  is then defined as the weighted summation of these transformed gates:  $G = \sum_{i=1}^{\alpha} p_i G_i$ .

An insightful observation can be made that in the presence of  $k$  occurrences of  $G$  gates within the circuit, the total count of possible arrangements aggregates to  $\alpha^k$ . These arrangements are uniquely labeled by the index  $q = \{1, 2, \dots, \alpha^k\}$ . As a result, this algorithm effectively dissects the trace  $\text{Tr}\{G^k\}$  of the higher-order powers of  $G$  into computations encompassing  $\alpha^k$  arrangements denoted as  $\mathcal{G}_q^k$ . The calculation process is thereby executed on higher-order mixed quantum states via the application of a Monte Carlo methodology.

The corresponding probability combination  $\prod_{t=1}^k p_{q_t}$  is represented as  $\mathcal{P}_q$ . Therefore,  $\text{Tr}\{G^k\}$  can be expressed as:

$$\text{Tr}\{G^k\} = \sum_{q=1}^{\alpha^k} \mathcal{P}_q \text{Tr}\{\mathcal{G}_q^k\}, \quad (17)$$

Where we use  $\mathcal{G}_q^k$  to denote  $\prod_{t=1}^k G_{q_t}$  for convenience.

## 2. The matrix representation of $\mathcal{G}_q^k$

For each of the  $\alpha^k$  instances of  $\mathcal{G}_q^k$ , a specific  $\mathcal{G}_q^k$  is chosen for computation where  $q = 1, 2, \dots, \alpha^k$ . In this scenario, the calculation method is provided for arbitrary combinations, while the computation process remains similar for other combinations.

Upon choosing a specific combination  $\mathcal{G}_q^k$ , a set of  $k$  corresponding  $G_{q_t}$  gates is determined, thereby giving rise to  $k$  specific  $|\psi_{q_t}\rangle$  states, where  $k \leq 2^n$  and  $t = 1, 2, \dots, k$ .

For example, consider the cases:

$$q = 1, \{\mathcal{G}_1^k : \underbrace{G_1 G_1 \cdots G_1 G_1}_{k \text{ layers}}\}.$$

$$q = 2, \{\mathcal{G}_2^k : \underbrace{G_1 G_1 \cdots G_1 G_2}_{k \text{ layers}}\}.$$

⋮

$$q = \alpha^k, \{\mathcal{G}_{\alpha^k}^k : \underbrace{G_\alpha G_\alpha \cdots G_\alpha G_\alpha}_{k \text{ layers}}\}.$$

Therefore, under the matrix background denoted as  $\mathcal{G}_q^k$ , the subspace dimension  $d$  is not constant. Hence, the determination of the subspace dimension relies entirely on the count of unique gate types present in the given order  $q$ . Let us define  $d$  as the dimension of the non-trivial subspace corresponding to the simplified merge of  $\mathcal{G}_q^k := \prod_{t=1}^k G_{q_t}$ , while representing the random gate sets used to prepare  $G_{q_t}$  as  $U_{q_t}$ :  $G_{q_t} = U_{q_t} G_0 U_{q_t}^\dagger$ . Furthermore, among the total  $k$  random gates, only  $d$  distinct

types exist. Quantum states prepared by different random gates are represented as:  $|\psi_{q_\zeta}\rangle, \zeta = 1, 2, \dots, d$ .

In order to ensure completeness, a set of state vectors  $\{|\phi_\eta\rangle, \eta = 1, 2, \dots, 2^n - d\}$  is introduced, which are orthogonal to all the state vectors  $|\psi_{q_\zeta}\rangle$ .

The rationale behind this is as follows:

Due to the condition  $\langle \psi_{q_\zeta} | \phi_\eta \rangle = 0$ , it can be inferred that:

$$\mathcal{G}_q^k(|\phi_\eta\rangle) = \left[ \prod_{\zeta=1}^d (I - 2(\langle \psi_{q_\zeta} | \psi_{q_\zeta} \rangle)) \right] |\phi_\eta\rangle = |\phi_\eta\rangle. \quad (18)$$

It is evident that  $\{|\phi_\eta\rangle, \eta = 1, 2, \dots, 2^n - d\}$  forms a set of eigenstates of  $\mathcal{G}_q^k$  with eigenvalue 1. In the representation with  $2^n$  state vectors:

$$\left\{ \underbrace{|\psi_{q_1}\rangle, |\psi_{q_2}\rangle, \dots, |\psi_{q_d}\rangle}_{d \text{ terms}}, \underbrace{|\phi_1\rangle, |\phi_2\rangle, \dots, |\phi_{2^n-d}\rangle}_{(2^n-d) \text{ terms}} \right\}. \quad (19)$$

as the basis in the  $V_q$  space, the matrix  $\mathcal{G}_q^k$  can be expressed as:

$$\begin{pmatrix} w_{11} & w_{12} & \dots & w_{1d} & 0 & 0 & \dots \\ w_{21} & w_{22} & \dots & w_{2d} & 0 & 0 & \dots \\ \dots & \dots & \dots & \dots & 0 & 0 & \dots \\ w_{d1} & w_{d2} & \dots & w_{dd} & 0 & 0 & \dots \\ 0 & 0 & 0 & 0 & 1 & 0 & \dots \\ 0 & 0 & 0 & 0 & 0 & \dots & \dots \\ \dots & \dots & \dots & \dots & \dots & \dots & 1 \end{pmatrix} \quad (20)$$

The top-left  $d \times d$  matrix  $w_q$  can be considered as composed of the eigenvalues of the  $d$ -dimensional invariant subspace  $V_{q1}$  spanned by  $d$  states  $|\psi_{q_\zeta}\rangle$  in the basis. The remaining part of  $\mathcal{G}_q^k$  is composed of the eigenvectors in the complement space with basis  $|\phi_\eta\rangle$ , corresponding to  $(2^n - d)$  eigenvalues. These eigenvalues form an  $(2^n - d) \times (2^n - d)$  identity matrix  $I_{(2^n-d) \times (2^n-d)}$ . Therefore,  $w_q$  is actually the matrix representation of  $\mathcal{G}_q^k$  in the  $d$ -dimensional invariant subspace  $V_{q1}$ . Through this expression, the calculation of  $\text{Tr}\{\mathcal{G}_q^k\}$  can be performed:

$$\begin{aligned} \text{Tr}\{\mathcal{G}_q^k\} &= \text{Tr}\{w_q\} + \text{Tr}\{I_{2^n-d}\} \\ &= \text{Tr}\{w_q\} + 2^n - d. \end{aligned} \quad (21)$$

## 3. The PTM representation of $w_q$

After characterizing  $\mathcal{G}_q^k$ , we need to obtain the solution for  $\text{Tr}\{w_q\}$ . However, the matrix  $w_q$  is unknown.  $w_q$  as a mapping, finding the solution for  $w_q$  requires the use of the Pauli Transfer Matrix(PTM). We denote the PTM corresponding to  $w_q$  as  $R_{w_q}$ .

Based on the previous discussion, an important relationship can be used:

$$R_{w_q} |\rho_s\rangle \rangle = |w_q(\rho_s)\rangle \rangle = |w_q \rho_s w_q^\dagger\rangle \rangle \quad (22)$$

$$r, s \in \{1, 2, \dots, d^2\}.$$

For simplicity, the subscript  $q$  indicating that  $\rho$  belongs to the ordering  $\mathcal{G}_q^k$  will be omitted below.

Although  $R_{w_q}$  is an  $(d^2 \times d^2)$  matrix, the vector  $|\rho_s\rangle\rangle$  has dimensions of  $(2^n)^2 \times 1$ . Since  $|\rho_s\rangle\rangle$  only has non-zero elements in the  $d^2$ -dimensional subspace, the remaining part of the vector is trivial, consisting of all zeros except for this subspace.

By left-multiplying the above equation by  $\langle\langle\rho_r|$ , the matrix elements of the *PTM* matrix  $(R_{w_q})_{d^2 \times d^2}$  are given as follows:

$$\langle\langle\rho_r|R_{w_q}|\rho_s\rangle\rangle = \langle\langle\rho_r|w_q\rho_sw_q^\dagger\rangle\rangle. \quad (23)$$

To calculate the matrix elements  $(R_{w_q})_{rs}$  of  $R_{w_q}$  using this method,  $d^2$  quantum states in the Hilbert-Schmidt space are required, represented by vectors  $|\rho_r\rangle\rangle$ . The proof of the completeness of these states can be found in Appendix A.

#### 4. GST

In Quantum Process Tomography (QPT), the information required to reconstruct each gate  $R_{w_q}$  is contained in the measurements of  $\langle\langle\rho_r|R_{w_q}|\rho_s\rangle\rangle$ , and  $R_{w_q}$  is the PTM of  $w_q$  in the Hilbert-Schmidt space. QPT assumes that the initial state and final measurements are known. In practice, these states and measurements must be prepared using quantum gates, and these gates  $\{F_r, F'_s\}$  themselves may have imperfections [40]:

$$\langle\langle\rho_r| = \langle\langle 0|F_r, \quad (24)$$

$$|\rho_s\rangle\rangle = F'_s|0\rangle\rangle. \quad (25)$$

Indeed, the initial states and final measurements that were prepared using gates are not directly known and can introduce errors in the estimation process. GST aims to characterize the fully unknown set of gates and states[45].

$$\mathcal{R} = \{|\rho\rangle\rangle, \langle\langle E|, R_{w_1}, \dots, R_{w_q}, \dots\}, q = 1, 2, \dots, \alpha^k. \quad (26)$$

GST has similar requirements to QPT: the ability to measure the set of gates  $\mathcal{R} = \{|\rho\rangle\rangle, \langle\langle E|, R_{w_1}, \dots, R_{w_{\alpha^k}}\}$  in the form of expectation values:

$$p = \text{Tr}\{\rho_r^\dagger w_q(\rho_s)\} = \langle\langle\rho_r|R_{w_q}|\rho_s\rangle\rangle = \text{Tr}\{\rho_r^\dagger w_q\rho_s w_q^\dagger\}. \quad (27)$$

To simplify the expression, we use  $\{F_r, F'_s\}$ , where  $(r, s = 1, 2, \dots, d^2)$ , to denote the quantum gates used for preparing quantum states and measurements, which are  $\{G_{qr}(\theta_r)U_{qr}\}$  and  $\{U_{qs}^\dagger G_{qs}^\dagger(\theta_s)\}$ , respectively. The density matrices of these prepared quantum states are linearly independent. Please refer to Appendix A for details. By constructing a quantum circuit, it is possible to compute the  $d^2$  matrix elements of the PTM matrix  $R_{w_q}$ . We define  $(R_{w_q})_{rs}$  as follows:

$$(R_{w_q})_{rs} = \langle\langle\rho_r|R_{w_q}|\rho_l\rangle\rangle = \langle\langle 0|F_r R_{w_q} F_s|0\rangle\rangle. \quad (28)$$

Inserting the completeness state into it yields:

$$\begin{aligned} p_{rs} &= (R_{w_q})_{rs} = \langle\langle\rho_r|R_{w_q}|\rho_s\rangle\rangle \\ &= \langle\langle 0|F_r R_{w_q} F_s|0\rangle\rangle \\ &= \sum_{a,b} \langle\langle 0|F_r|a\rangle\rangle \langle\langle a|R_{w_q}|b\rangle\rangle \langle\langle b|F_s|0\rangle\rangle \\ &= \sum_{a,b} A_{ra}(R_{w_q}) B_{bs}. \end{aligned} \quad (29)$$

It can be easily verified that:

$$\begin{aligned} p_{rs} &= (AR_{w_q}B)_{rs}, \\ A &= \sum_r |r\rangle\rangle \langle\langle 0|F_r, \\ B &= \sum_s F_s|0\rangle\rangle \langle\langle s|. \end{aligned} \quad (30)$$

Let  $\tilde{R}_{w_q} = AR_{w_q}B$ , the identity matrix  $I$  also serves as a mapping, and its PTM has the following properties:

$$R_I|\rho_s\rangle\rangle = |I(\rho_s)\rangle\rangle = |I\rho_s I^\dagger\rangle\rangle = |\rho_s\rangle\rangle. \quad (31)$$

It can be observed that the action of  $R_I$  is similar to the identity matrix and its matrix elements can be expressed as follows:

$$(R_I)_{rs} = \langle\langle\rho_r|R_I|\rho_s\rangle\rangle = \text{Tr}\{\rho_r^\dagger I \rho_s I^\dagger\} = \text{Tr}\{\rho_r^\dagger \rho_s\}. \quad (32)$$

Denoting  $g_{rs} = (R_I)_{rs} = \langle\langle\rho_r|\rho_s\rangle\rangle = \langle\langle 0|F_r F_s|0\rangle\rangle$ , we can insert the completeness state and obtain:

$$g_{rs} = \sum_{a,b} \langle\langle 0|F_r|a\rangle\rangle \langle\langle a|b\rangle\rangle \langle\langle b|F_s|0\rangle\rangle = (AB)_{rs}. \quad (33)$$

For a given combination  $\mathcal{G}_q^k$ , let  $\tilde{R}_{I_q} = AB$ , where  $A$  and  $B$  are matrices. The experimental measurement value  $p_{rs}$  corresponds to the  $rs$  component of the matrix  $A(R_{w_q})B$ , while  $g_{rs}$  corresponds to the  $rs$  component of the matrix  $(AB)$ . The quantum channel we reconstruct will differ from the real quantum channel by a similarity transformation:

$$(\tilde{R}_I)^{-1} \tilde{R}_{w_q} = B^{-1} A^{-1} A R_{w_q} B = B^{-1} R_{w_q} B. \quad (34)$$

Therefore, we can estimate the trace of  $R_{w_q}$ :

$$\text{Tr}\{(\tilde{R}_I)^{-1} \tilde{R}_{w_q}\} = \text{Tr}\{B^{-1} R_{w_q} B\} = \text{Tr}\{R_{w_q}\}. \quad (35)$$

Based on the calculations mentioned earlier, the value of  $\text{Tr}\{R_{w_q}\} = |\text{Tr}\{w_q\}|^2$  can be determined. However, this is not the final result for  $\text{Tr}\{w_q\}$ .

Note: In order to avoid ill-conditioned matrices  $R_{I_q}$ , it is necessary to perform subspace selection. For detailed analysis, please refer to Section IV A.

### 5. Mathematical Processing of Results

To calculate  $Tr\{w_q\}$ , an operation involving taking the square root is required:  $|Tr\{w_q\}|^2 = Tr\{R_{w_q}\}$ . In general,  $Tr\{w_q\}$  can be decomposed into real and imaginary parts:

$$Tr\{w_q\} = Re[Tr\{w_q\}] + i \cdot Im[Tr\{w_q\}]. \quad (36)$$

then

$$Tr\{R_{w_q}\} = (Re[Tr\{w_q\}])^2 + (Im[Tr\{w_q\}])^2. \quad (37)$$

In fact, only the real part needs to be estimated because the sum of all the imaginary parts of  $Tr\{w_q\}$  vanishes after summation.

$$\sum_{q=1}^{\alpha^k} Tr\{w_q\} = \sum_{q=1}^{\alpha^k} Re[Tr\{w_q\}]. \quad (38)$$

Next, we show how to estimate the real part of  $Tr\{w_q\}$ . Consider  $(w'_q)_{d+1} = (w_q)_d \oplus I_1$ , where  $w'_q$  is the representation of  $\mathcal{G}_q^k$  on the subspace  $V'_q := \text{span}\{|\psi_{q_1}\rangle, |\psi_{q_2}\rangle, \dots, |\psi_{q_d}\rangle, |\phi_1\rangle\}$ .

$$w'_q = \begin{pmatrix} w_q & 0 \\ 0 & 1 \end{pmatrix} \quad (39)$$

It can be seen that  $V'_q$  is also a noninvariant subspace of  $\mathcal{G}_q^k$ . It's obvious that

$$Tr\{w'_q\} = Tr\{w_q\} + 1, \quad (40)$$

and:

$$\begin{aligned} Tr\{R_{w'_q}\} &= |Tr\{w'_q\}|^2 = |Tr\{w_q\} + 1|^2 \\ &= |Re[Tr\{w_q\}] + i \cdot Im[Tr\{w_q\}] + 1|^2 \\ &= (Re[Tr\{w_q\}])^2 + 2(Re[Tr\{w_q\}]) \\ &\quad + (Im[Tr\{w_q\}])^2 + 1. \end{aligned} \quad (41)$$

Recall the relation

$$\begin{aligned} Tr\{R_w\} &= |Tr\{w_q\}|^2 \\ &= (Re[Tr\{w_q\}])^2 + (Im[Tr\{w_q\}])^2, \end{aligned} \quad (42)$$

we can find that

$$Re[Tr\{w_q\}] = \frac{1}{2}[Tr\{R_{w'_q}\} - Tr\{R_{w_q}\} - 1]. \quad (43)$$

The procedure to calculate  $Tr\{R_{w'_q}\}$  follows a similar algorithm as for computing  $Tr\{R_{w_q}\}$ , with the distinction that in this case,  $(d+1)^2$  quantum states are required.

### B. Algorithm Process of Tomography

The following is the procedure for calculating  $Tr\{\rho^m\}$  for the quantum state  $\rho = \sum_{i=1}^{\alpha} p_i U_i |0\rangle\langle 0| U_i^\dagger$ .

#### Main Program:

1. Set the initial state as  $|0\rangle^{\otimes n}$ , utilize  $\alpha$  randomly chosen gates to prepare quantum states  $\rho_i$  individually. Subsequently, perform a linear correlation analysis on the corresponding  $|\rho_i\rangle\rangle$  states. By comparing the eigenvalues of their Gram matrix with the predefined threshold  $\epsilon$ , the dimension  $D = d_{MAX}$  of the subspace is determined. For further details, refer to Section IV A .
2. With a probability of 1/2, apply a  $G$  gate in the circuit; and with a probability of 1/2, apply an  $I$  gate in the circuit. Sample this process for a total of  $m$  times to generate a sequence of gates that includes both  $G$  and  $I$  gates. Let's assume that in a single sampling instance, there were  $k$  occurrences of  $G$  gates and  $(m-k)$  occurrences of  $I$  gates, where  $k \in \{1, 2, \dots, m\}$ . The case where  $k = 0$  can be directly computed and is omitted.
3. For  $k \in \{1, 2, \dots, m\}$ , select  $\mathcal{G}_q^k$  with probability  $\mathcal{P}_q$ , and invoke a subroutine to calculate  $Tr\{\mathcal{G}_q^k\}$  within its corresponding subspace of dimension  $d$ . Here,  $\mathcal{P}_q = \prod_{t=1}^k p_{q_t}$  and  $\mathcal{G}_q^k = \prod_{t=1}^k G_{q_t}$ .
4. Repeat the above steps  $N$  times and then calculate the average.

$$\begin{aligned} Tr\{(\frac{1}{2}I - \frac{1}{2}G)^m\} &= \sum_{k=0}^m (\frac{1}{2})^m (-1)^{m-k} Tr\{G^k\} \\ &= \sum_{k=0}^m p_k x_k. \end{aligned}$$

Where:  $p_k = \frac{1}{2}^m C_m^k$ ,  $x_k = (-1)^{m-k} Tr\{G^k\}$ . Run the process  $N$  times, calculate the results, sum up, and then divide by  $N$  to estimate  $E(x_k) = Tr\{\rho^m\}$ .

#### Subroutine:

The following is the calculation of  $Tr\{\mathcal{G}_q^k\}$ , where  $k \in \{1, 2, \dots, m\}$ ;  $q \in \{1, 2, \dots, \alpha^k\}$ . The case of  $k = 0$  can be computed directly, thus making  $k$  range from 1 to  $m$ .

1. For  $\mathcal{G}_q^k$ , there is a corresponding relation:  $\mathcal{G}_q^k \sim w_q \sim R_{w_q}$ , where  $\mathcal{G}_q^k := G_{q_1} \cdot G_{q_2} \cdots G_{q_t} \cdots G_{q_k}$ ;  $t \in \{1, 2, \dots, k\}$ . The corresponding random gate sequence  $U_{q_1} \cdot U_{q_2} \cdots U_{q_t} \cdots U_{q_k}$ ;  $w_q$  is the representation of  $\mathcal{G}_q^k$  in the nontrivial invariant subspace and  $R_{w_q}$  is the Pauli transfer matrix of  $w_q$ .
2. Determine the dimension  $d \leq d_{MAX}$  of the subspace  $V_{q_1}$  corresponding to  $\mathcal{G}_q^k$ , then prepare  $d$  linearly independent quantum states:  $(\zeta \in$

$\{1, 2, \dots, d\}$

$$\rho_{q_\zeta} = |\psi_{q_\zeta}\rangle\langle\psi_{q_\zeta}| = U_{q_\zeta}|0\rangle\langle 0|U_{q_\zeta}^\dagger.$$

3. Utilize  $G_{\zeta'}(\theta_{\zeta'})$ , ( $\theta_{\zeta'} \neq Z\pi$ ) to prepare  $(d^2 - d)$  additional quantum states, in conjunction with step 2 of the Subroutine, to form a total of  $d^2$  linearly independent quantum states.

$$\begin{aligned} \rho_{q_{\zeta'}} &= |\psi_{q_{\zeta'}}\rangle\langle\psi_{q_{\zeta'}}| \\ &= G_{\zeta'}(\theta_{\zeta'})U_{q_\zeta}|0\rangle\langle 0|U_{q_\zeta}^\dagger G_{\zeta'}^\dagger(\theta_{\zeta'}), \\ \zeta' &\in \{1, 2, \dots, d\} \text{ and } \zeta' \neq \zeta. \end{aligned}$$

4. The  $d^2$  quantum states are uniformly denoted as  $\{\rho_r, \rho_s; r, s = 1, 2, \dots, d^2\}$ . Traverse the prepared quantum states  $\rho_s$  cyclically and implement the quantum object of interest  $\mathcal{G}_q^k$  in the circuit. Then, add the measurement  $\rho_r^\dagger$ :

$$|\psi_s\rangle \xrightarrow{\boxed{\mathcal{G}_q^k}} \langle\psi_r|$$

where:  $r, s \in \{1, 2, \dots, d^2\}$ , indicating the iteration over all quantum states  $\{\rho_i\}$ , with the subsequent quantum state  $\rho_r^\dagger$  chosen as the measurement operator. This results in:  $(\tilde{R}_{w_q})_{r,s} = (AR_{w_q}B)_{r,s}$

5. Iterate through all quantum states  $\{\rho_i\}$  and perform the following computation in the circuit:

$$|\psi_s\rangle \xrightarrow{\boxed{I}} \langle\psi_r|$$

Similarly, using  $\rho_r^\dagger$  as the measurement operator, the matrix  $(\tilde{R}_I)_{r,s} = (AR_IB)_{r,s} = (AB)_{r,s}$  is obtained.

6. Compute  $Tr\{(\tilde{R}_I^{-1} \cdot \tilde{R}_{w_q})\} = Tr\{BR_{w_q}B^{-1}\} = Tr\{R_{w_q}\}$ .

7. Expand the subspace  $V_{q1} \rightarrow V'_q$  to achieve a dimension of . For more detailed information, please refer to Section IIIA4. The corresponding PTM is denoted as  $R_{w'_q}$ . Then, employ the process outlined in steps 4-10 to calculate  $Tr\{R_{w'_q}\}$ .

8. Utilize

$$\text{Re}[\text{Tr}\{w_q\}] = \frac{1}{2} [\text{Tr}\{R_{w'_q}\} - \text{Tr}\{R_{w_q}\} - 1],$$

to calculate all  $\text{Re}[\text{Tr}\{w_q\}]$  corresponding to each  $q$ , iterating through all  $q$ .

## IV. ERROR ANALYSIS

### A. Eigenvalue Truncation of the simplest case

To prevent the introduction of significant statistical errors during subsequent numerical computations, it becomes imperative to truncate the eigenvalues of the Gram

matrix  $g$ . In order to ensure that the eigenvalues of the Gram matrix are all greater than threshold  $\epsilon$ , we start from  $|\psi_2\rangle$  to select the quantum states that constitute the subspace. Here we default to  $|\psi_1\rangle$  in the subspace,

Commencing from the iteration  $k = 2$ , the computation of the Gram matrix  $g_k$  is carried out. This matrix is associated with four distinct eigenvectors, which can be identified as follows:

$$|\Psi_1\rangle\langle\Psi_1|, |\Psi_1\rangle\langle\Psi_2|, |\Psi_2\rangle\langle\Psi_1|, |\Psi_2\rangle\langle\Psi_2|. \quad (44)$$

where  $|\Psi_1\rangle = |\psi_1\rangle$  and  $|\Psi_2\rangle$  is defined from the Schmidt orthogonalization.

$$|\Psi_2\rangle = \frac{1}{\Delta_2}|\psi_2\rangle - \frac{x_{1,1}}{\Delta_2}|\psi_1\rangle. \quad (45)$$

Here  $x_{1,1}$  is the overlap  $\langle\psi_1|\psi_2\rangle$  and  $|\Delta_2|^2 = 1 - |x_{1,1}|^2$  is a normalization factor. The eigenvalues are respectively given by

$$1, \frac{|\Delta_2|^2}{1 + |x_{1,1}|^2}, \frac{|\Delta_2|^2}{1 + |x_{1,1}|^2}, |\frac{|\Delta_2|^2}{1 + |x_{1,1}|^2}|^2. \quad (46)$$

If the smallest eigenvalue  $|\frac{|\Delta_2|^2}{1 + |x_{1,1}|^2}|^2$  is smaller than the threshold  $\epsilon$  we pre-set, we add  $|\psi_2\rangle$  into the subspace. If not, we discard  $|\psi_2\rangle$  and then consider whether  $|\psi_3\rangle$  can be added into the subspace.

### B. eigenvalue truncation for general cases

We generalize the discussion in the previous subsection to the case of a higher dimensional subspace. Assume that the current subspace already contains  $|\psi_1\rangle, \dots, |\psi_{k-1}\rangle$ , and now we need to decide whether we want to add  $|\psi_k\rangle$  to the subspace.  $|\psi_k\rangle$  can be written as:

$$|\psi_k\rangle = \sum_i^{k-1} x_{k,i}|\psi_i\rangle + \Delta_k|\Psi_k\rangle, \quad (47)$$

where

$$|\Psi_k\rangle = \frac{1}{\Delta_k}|\psi_k\rangle - \frac{1}{\Delta_k}\sum_i^{k-1} x_{k,i}|\psi_i\rangle. \quad (48)$$

In this case, the smallest singular value is  $|\frac{|\Delta_k|^2}{1 + |x_k|^2}|^2$ , where  $|x_k|^2 = \sum_i^{k-1} |x_{k,i}|^2$ .

We must assess the relationship between the smallest singular value and  $\epsilon$ . If the smallest eigenvalue surpasses  $\epsilon$ , we should proceed with enlarging the subspace. However, if the smallest singular value is less than  $\epsilon$ , it is advisable to disregard the state  $|\psi_k\rangle$ .

### C. Eigenvalue Estimation Error

In the actual process, the measurement of the Gram matrix has statistical errors  $\Delta(g)$ . This will lead to errors

in the calculation of the eigenvalues of the Gram matrix. Given that each element of  $\Delta(g)$  is subjected to measurement  $N$  times, it follows that every element holds an order of magnitude around  $O\left(\frac{1}{\sqrt{N}}\right)$ . By referencing the Disk Theorem, no eigenvalue surpasses the scale of  $O\left(\frac{d^2}{\sqrt{N}}\right)$ . Applying the Weyl inequality[46] allows us to deduce that the disparity between the computed minimum eigenvalue of  $g$  and the actual minimum eigenvalue doesn't exceed  $O\left(\frac{d^2}{\sqrt{N}}\right)$ . Employing Hoeffding's inequality, the likelihood of each element within  $\Delta(g)$  being less than  $\tilde{\epsilon}_g$  amounts to  $1 - \delta_g < 1 - 2e^{-2N\tilde{\epsilon}_g^2}$ . Consequently, the probability of every element being less than  $\tilde{\epsilon}_g$ , i.e., the error of the eigenvalue will not exceed  $d^2\tilde{\epsilon}_g$ , can be expressed as  $(1 - \delta_g)^{d^2} > 1 - d^2\delta_g = 1 - \tilde{\delta}_g$ , Where

$$\tilde{\delta}_g = d^2\delta_g \geq 2d^2e^{-2N\tilde{\epsilon}_g^2}. \quad (49)$$

This means that the solution for eigenvalues, to achieve precision  $d^2\tilde{\epsilon}_g$  with a probability of  $1 - d^2\tilde{\delta}_g$ , does not require more measurements than

$$N = O\left(\frac{\log \frac{d^2}{\tilde{\delta}_g}}{\tilde{\epsilon}_g^2}\right), \quad (50)$$

for each matrix element.

#### D. The error analysis of $g^{-1}$

In the GST process, we need to invert the gram matrix. Next, we consider the effect of the error  $\Delta(g)$  on the trace of the inversion. Using Taylor expansion,

$$(g + \Delta(g))^{-1} = g^{-1} - g^{-1}\Delta(g)g^{-1} + g^{-1}\Delta(g)g^{-1}\Delta(g)g^{-1} + \dots \quad (51)$$

The trace of each term can be bounded as

$$Tr\{g^{-1}\} < \frac{d}{\epsilon}. \quad (52)$$

$$Tr\{g^{-1}\Delta(g)g^{-1}\} < \frac{d^2\tilde{\epsilon}_g}{\epsilon^2}. \quad (53)$$

$$Tr\{(g^{-1}\Delta g)^k g^{-1}\} < \frac{d^{2k}\tilde{\epsilon}_g^k}{\epsilon^{k+1}}. \quad (54)$$

let  $\tilde{\epsilon}_g = \epsilon_1\epsilon^2$ , then :

$$Tr\{g^{-1} - (g + \Delta(g))^{-1}\} < d^2\epsilon_1 + d^2\epsilon_1 \times d^2\epsilon_1\epsilon + (d^2\epsilon_1)(d^2\epsilon_1\epsilon)^2 + \dots, \quad (55)$$

which can be bounded as

$$Tr\{g^{-1} - (g + \Delta(g))^{-1}\} < \frac{d^2\epsilon_1}{1 - d^2\epsilon}. \quad (56)$$

This shows that the estimation of the inverse of the gram matrix will not exceed

$$N_1 = O\left(\frac{d^4 \log \frac{d^2}{\tilde{\delta}_g}}{\epsilon_1^2 \epsilon^4}\right). \quad (57)$$

for each term of the gram matrix to achieve accuracy  $\frac{d^2\epsilon_1}{1 - d^2\epsilon}$  with the probability of  $1 - d^2\tilde{\delta}_g$

#### E. Sampling Error

In this section, we consider the statistical error when finding the trace of a quantum gate. Let  $(R_{w_y})_{i,j} = \langle \langle \rho_i | G | \rho_j \rangle \rangle$ . The error in computing  $Tr\{g^{-1}R_{w_y}\}$  is given by:

$$Tr\{\Delta(g^{-1})R_{w_y}\} + Tr\{g^{-1}\Delta(R_{w_y})\} + Tr\{\Delta(g^{-1})\Delta(R_{w_y})\}. \quad (58)$$

The first term can be bounded as

$$Tr\{\Delta(g^{-1})R_{w_y}\} = Tr\{g^{-1} - (g + \Delta(g))^{-1}\} < d^3\epsilon_1, \quad (59)$$

The second term is

$$Tr\{g^{-1}\Delta(R_{w_y})\} < \frac{d^2\epsilon_2}{\epsilon}, \quad (60)$$

where we have used

$$Tr\{\Delta(R_{w_y})\} < d\epsilon_2. \quad (61)$$

The last term is

$$Tr\{\Delta(g^{-1})\Delta(R_{w_y})\} < d^2\epsilon_1\epsilon_2. \quad (62)$$

So all the terms must add up to less than

$$d^3\epsilon_1 + \frac{d^2\epsilon_2}{\epsilon} + d^2\epsilon_1\epsilon_2. \quad (63)$$

According to Hoeffding's inequality, the probability that one of the terms in  $\Delta(R_{w_y})$  is less than  $\epsilon_2$  is  $1 - \delta_m > 1 - 2e^{-2N_m\epsilon_m^2}$ . Therefore, the probability that each term is less than  $\tilde{\epsilon}_g$  is  $(1 - \delta_m)^{d^2} > 1 - d^2\delta_m = 1 - \tilde{\delta}_m$ .

Therefore, The matrix elements of a quantum gate do not require more measurements than

$$N_m = O\left(\frac{\log \frac{d^2}{\tilde{\delta}_m}}{\tilde{\epsilon}_2^2}\right). \quad (64)$$

#### F. Truncation Error

Unlike the error caused by statistical fluctuations, truncation error emerges from the omission of specific quantum states during the subspace construction. We analyze disparities between two quantum circuits: one denoted as  $G$ , representing the implemented circuit

within our setup, and the other denoted as  $G'$ , derived by substituting a gate layer in  $G$ . Specifically,  $G = G_1 G_2 G_3 \cdots G_n$  constitutes an  $n$ -layer gate circuit corresponding to states  $|\psi_1\rangle, |\psi_2\rangle, \dots, |\psi_n\rangle$ . During subspace construction, certain states like  $|\psi_k\rangle$  might be excluded. In the case of  $G'$ ,  $|\psi_k\rangle$  is replaced with  $|\psi'_k\rangle$ , effectively eliminating the constituent  $|\phi_k\rangle$ . To discard  $|\phi_k\rangle$ , a certain condition must be satisfied.

$$\left| \frac{|\epsilon_k|^2}{1 + |x_k|^2} \right|^2 < \epsilon. \quad (65)$$

In other words,  $\epsilon_k$  can be at most  $\epsilon^{1/4}$ . Since there is an error in estimating the eigenvalues of  $g$ , the maximum value of  $\epsilon_k$  is  $\epsilon_3 = (\epsilon + O(\frac{d^2}{\sqrt{N}}))^{1/4}$ . Therefore,  $|Tr\{G'\} - Tr\{G\}| \sim O(n\epsilon_3)$ . Since we discard at most  $n$  states  $|\phi_j\rangle$ , Then  $|Tr\{G'\}|^2 - |Tr\{G\}|^2 \sim O(n\epsilon_3)$ .

Let  $G$  and  $G'$  correspond to  $R_{w_y}$  and  $R'_{w_y}$ , respectively. Then we have  $|Tr\{R'_{w_y}\} - Tr\{R_{w_y}\}| \sim O(dn\epsilon_3)$ .

Based on the eigenvalue estimation error, the number of measurements satisfies:

$$N_1 = O\left(\frac{\log \frac{d^2}{1\delta_g}}{\tilde{\epsilon}_g^2}\right). \quad (66)$$

Then,  $\epsilon_3 < (\epsilon + \tilde{\epsilon}_g)^{1/4}$ .

## V. NUMERICAL SIMULATION

### A. Quantum state preparation

In the preceding text, we postulated that for the algorithm to be effective, knowledge of the mixed quantum state's preparation method is imperative. To ensure universality, we express any single-qubit gate through a combination of three fundamental rotation gates. Thus, in this paper, we opt for the  $U(\theta, \phi, \lambda)$  gate as the random gate to prepare the mixed quantum state, allowing us to perform computations using both methods and subsequently compare the outcomes.

The three basic rotation gates are rotations around the **X**, **Y**, and **Z** axes:

$$U(\theta, \phi, \lambda) = \begin{pmatrix} \cos(\theta/2) & -e^{i\lambda} \sin(\theta/2) \\ e^{i\phi} \sin(\theta/2) & e^{i\lambda+i\phi} \cos(\theta/2) \end{pmatrix} \quad (67)$$

where  $\theta$ ,  $\phi$ , and  $\lambda$  are real numbers, and  $i$  is the imaginary unit. By encoding this general parameterized gate into a single-qubit quantum gate in the quantum circuit, an  $n$ -qubit gate can be obtained through tensor product operation:  $U^{\otimes n}$ . Different quantum states are prepared by using various quantum gates, and then a quantum mixed state is simulated by employing a probability-weighted method.

### B. Processing of the calculation results of the Hadamard Test

The random gates we need are denoted as  $U_{y_s}$ , where  $s = 1, 2, \dots, k + 1$ ,  $y_s \in \{1, 2, 3, 4\}$ . The probability of the random gate  $U_{y_s}$  is denoted by  $p_{y_s}$ . Let  $U_{y_s} = U(\theta_{y_s}, \phi_{y_s}, \lambda_{y_s})$ . To simulate the computation of  $Tr\{\rho^{k+1}\}$ , the circuit we construct is shown in Fig 3:

We iterate through  $y_s$  to obtain the corresponding  $P_y(0)$  for each set of  $U_{y_s}$ . Summing up all these cases yields the overall  $\mathcal{P}(0)$ :

$$\mathcal{P}(0) = \sum_{y=1}^{\alpha^{k+1}} \left[ \prod_{s=1}^{k+1} p_{y_s} \right] P_y(0). \quad (68)$$

Similarly, by following the same procedure we can obtain

$$\mathcal{P}(1) = \sum_{y=1}^{\alpha^{k+1}} \left[ \prod_{s=1}^{k+1} p_{y_s} \right] P_y(1). \quad (69)$$

With Eq.(9) and Eq.(10), we can deduce  $Tr\{G^k \rho\}$ , subsequently leading us to the derivation of  $Tr\{\rho^{m+1}\}$ .

### C. Obtaining the data and exploring potential applications

In this study, the random gates in the circuit are simulated by selecting different parameters for  $U(\theta, \phi, \lambda)$ . For generality, the parameter selection is based on random numbers. The parameters for the random gates used in this study are shown in Table I. The probabilities for the four random gates are 0.1, 0.2, 0.3, and 0.4. Based on the above content, the values of  $Tr\{\rho^m\}$  obtained using two different methods are shown in Table II.

From the analysis of the data above, we can see that the numerical values of  $Tr\{\rho^m\}$  obtained using the HT

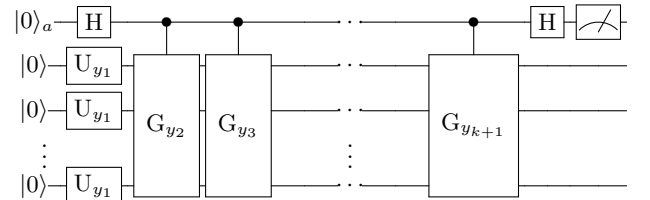


FIG. 3. 4-qubits Quantum Circuit: The first line represents an ancillary circuit, with the initial state set to  $|0\rangle_a$ . It then undergoes a Hadamard gate, resulting in a superposition state. The three lines below represent the preparation and measurement of the target quantum states, with initial states all set to  $|0\rangle$ . After applying the first random gate  $U_{y_1}$ , the target quantum state  $\rho_{y_1} = U_{y_1}|0\rangle\langle 0|U_{y_1}^\dagger$  is obtained through tensor product. Next, controlled quantum gates  $G_{y_2}, G_{y_3} \cdots G_{y_{k+1}}$  are applied, followed by another Hadamard gate on the ancillary circuit. Finally, measurement in the computational basis is performed on the ancillary circuit.

TABLE I. The values of the parameters

	$\theta_{y_s}$	$\phi_{y_s}$	$\lambda_{y_s}$
i=1	$0.29\pi$	$0.07\pi$	$0.11\pi$
i=2	$0.46\pi$	$0.62\pi$	$0.82\pi$
i=3	$0.41\pi$	$0.59\pi$	$0.53\pi$
i=4	$0.55\pi$	$0.31\pi$	$0.60\pi$

\* The parameters of the random gates used to generate the above data.

and GST are very close. More data considering shot noise can be found in Appendix B.

However, compared to HT, the GST method doesn't require an additional ancillary qubit, potentially reducing the implementation cost of the quantum circuit. This implies that practical applications could benefit from using fewer physical qubits and controlled gates, which is a critical factor to consider. Reducing the number of controlled gates could lower the error rate of the quantum circuit, thereby enhancing the system's reliability.

Based on the obtained  $Tr\{\rho^m\}$ , it is possible to calculate  $Tr\{\rho ln\rho\}$ ,  $Tr\{e^{\rho t}\}$ ,  $Tr\{e^{i\rho t}\}$ , etc. For example  $Tr\{\rho ln\rho\}$ : the expansion of  $\rho ln\rho$  with respect to  $G$  yields the following expression:

$$\rho ln\rho \approx -\frac{1}{2}ln2(I - G) - \frac{1}{2}G + \frac{1}{2}\left\{(1 - \frac{1}{2})G^2 + \left(\frac{1}{2} - \frac{1}{3}\right)G^3 + \dots + \left(\frac{1}{n-1} - \frac{1}{n}\right)G^n + \frac{1}{n}G^{n+1}\right\}. \quad (70)$$

For  $Tr\{\rho ln\rho\}$ , the theoretical value can be obtained using the method of matrix multiplication. However, after expansion, it can be calculated using the two methods described in this paper.

As shown in Table III, it's evident that as the power  $m$  increases, the theoretical and experimental values converge, yielding a diminishing relative error. Upon juxtaposing Table II, one can discern the remarkable similarity between the outcomes derived from both algorithms. Furthermore, by extending the power function analysis to the Renyi entropy and higher-order powers, we can gradually approximate the theoretical values of the density matrix's nonlinear functions. The code can be found in HT and GST.

TABLE II. The numerical value of the parameter

	Hadamard Test	Tomography
$Tr\{\rho^2\}$	0.650	0.650
$Tr\{\rho^3\}$	0.486	0.486
$Tr\{\rho^4\}$	0.375	0.375

\* The computational results obtained using the two algorithms in this article are presented with three decimal places.

TABLE III. Comparison between the calculated  $Tr\{\rho ln\rho\}$  using the method described in this paper and its theoretical value

	$Tr\{G^m\}$	T value	M value	RE
$m = 2$	6.600	-0.600	-0.569	5.17%
$m = 3$	5.914	-0.600	-0.543	9.50%
$m = 4$	6.066	-0.600	-0.574	4.30%
$m = 5$	5.814	-0.600	-0.573	4.50%
$m = 6$	5.830	-0.600	-0.582	3.00%
$m = 7$	5.726	-0.600	-0.583	2.83%
$m = 8$	5.710	-0.600	-0.586	2.33%

\* Note: **T-value** represents the theoretical value of  $Tr\{\rho ln\rho\}$ , and **M-value** represents the measured value of  $Tr\{\rho ln\rho\}$ . **RE** represents the relative error. The value of  $Tr\{G^m\}$  is measured using the method described in this article. The measured value of  $tr(\rho ln\rho)$  can be calculated using  $Tr\{G^m\}$ .

## VI. CONCLUSION

In this article, we present two algorithms for computing the power function of the density matrix by encoding the quantum state into a quantum channel. The first algorithm is based on the HT. In the absence of noise, this algorithm provides an unbiased estimate of the power function. However, it requires a significant number of control-G gates, which is not favorable for current hardware limitations. Therefore, we propose an alternative algorithm based on GST. The original GST is not scalable, but for our specific problem, we can perform GST only within the non-trivial subspace and extract the necessary information. The advantage of this algorithm lies in significantly reducing the utilization of two-qubit gates. Nevertheless, due to the need to mitigate the impact of shot noise on results, subspace selection introduces minor biases to the outcomes. As an example, we apply both methods to compute the von Neumann entropy of a randomly generated quantum state. It is worth noting that these algorithms can be used not only for computing the power function of the density matrix but also for evaluating nonlinear functions of physical quantities such as  $Tr\{O\rho^m\}$ .

## ACKNOWLEDGMENTS

This work is supported by National Natural Science Foundation of China (Grant No. 12225507, 12088101) and NSAF (Grant No. U1930403).

## VII. AUTHOR CONTRIBUTIONS

YRY conceived this work, and the three individuals collectively organized the ideas, clarified theoretical

knowledge, and contributed valuable thoughts and insights. ZWC and CTT constructed the circuits and con-

ducted data analysis, while YRY oversaw all the tasks. With the participation of all co-authors, this manuscript was written.

---

[1] T. D. Ladd, F. Jelezko, R. Laflamme, Y. Nakamura, C. Monroe, and J. L. O'Brien, *nature* **464**, 45 (2010).

[2] C. Monroe and J. Kim, *Science* **339**, 1164 (2013).

[3] M. H. Devoret and R. J. Schoelkopf, *Science* **339**, 1169 (2013).

[4] D. D. Awschalom, L. C. Bassett, A. S. Dzurak, E. L. Hu, and J. R. Petta, *Science* **339**, 1174 (2013).

[5] H. Bernien, S. Schwartz, A. Keesling, H. Levine, A. Omran, H. Pichler, S. Choi, A. S. Zibrov, M. Endres, M. Greiner, *et al.*, *Nature* **551**, 579 (2017).

[6] J. Preskill, *Quantum* **2**, 79 (2018).

[7] I. Y. Dodin and E. A. Startsev, arXiv preprint arXiv:2105.07317 (2021).

[8] Z. Holmes, N. J. Coble, A. T. Sornborger, and Y. Subaşı, *Physical Review Research* **5**, 013105 (2023).

[9] S. Subramanian and M.-H. Hsieh, *Physical review A* **104**, 022428 (2021).

[10] P. Horodecki, *Physical Review A* **68**, 052101 (2003).

[11] T. A. Brun, arXiv preprint quant-ph/0401067 (2004).

[12] K. Zyczkowski and I. Bengtsson, arXiv preprint quant-ph/0606228 (2006).

[13] B. Vermersch, A. Rath, B. Sundar, C. Branciard, J. Preskill, and A. Elben, arXiv preprint arXiv:2304.12292 (2023).

[14] A. Rath, C. Branciard, A. Minguzzi, and B. Vermersch, *Physical Review Letters* **127**, 260501 (2021).

[15] V. Vitale, A. Rath, P. Jurcevic, A. Elben, C. Branciard, and B. Vermersch, arXiv preprint arXiv:2307.16882 (2023).

[16] R. Jozsa, *Journal of modern optics* **41**, 2315 (1994).

[17] Q. Wang, J. Guan, J. Liu, Z. Zhang, and M. Ying, arXiv preprint arXiv:2203.13522 (2022).

[18] A. Kandala, A. Mezzacapo, K. Temme, M. Takita, M. Brink, J. M. Chow, and J. M. Gambetta, *nature* **549**, 242 (2017).

[19] B. Koczor, *Physical Review X* **11**, 031057 (2021).

[20] W. J. Huggins, S. McArdle, T. E. O'Brien, J. Lee, N. C. Rubin, S. Boixo, K. B. Whaley, R. Babbush, and J. R. McClean, *Physical Review X* **11**, 041036 (2021).

[21] K. Yamamoto, S. Endo, H. Hakoshima, Y. Matsuzaki, and Y. Tokunaga, *Physical Review Letters* **129**, 250503 (2022).

[22] M. Huo and Y. Li, *Physical Review A* **105**, 022427 (2022).

[23] H. A. Carteret, *Physical review letters* **94**, 040502 (2005).

[24] H. A. Carteret, arXiv preprint arXiv:1605.08751 (2016).

[25] A. Elben, R. Kueng, H.-Y. R. Huang, R. van Bijnen, C. Kokail, M. Dalmonte, P. Calabrese, B. Kraus, J. Preskill, P. Zoller, *et al.*, *Physical Review Letters* **125**, 200501 (2020).

[26] S. Lloyd, M. Mohseni, and P. Rebentrost, *Nature Physics* **10**, 631 (2014).

[27] M. Lubasch, J. Joo, P. Moinier, M. Kiffner, and D. Jaksch, *Physical Review A* **101**, 010301 (2020).

[28] B. Georgeot and D. L. Shepelyansky, *Physical Review Letters* **86**, 2890 (2001).

[29] B. Georgeot and D. Shepelyansky, *Physical Review Letters* **86**, 5393 (2001).

[30] Y. Zhou and Z. Liu, arXiv preprint arXiv:2208.08416 (2022).

[31] A. K. Ekert, C. M. Alves, D. K. Oi, M. Horodecki, P. Horodecki, and L. C. Kwek, *Physical review letters* **88**, 217901 (2002).

[32] S. H. Sack, R. A. Medina, A. A. Michailidis, R. Kueng, and M. Serbyn, *PRX Quantum* **3**, 020365 (2022).

[33] M. A. Nielsen and I. L. Chuang, *Quantum Computation and Quantum Information: 10th Anniversary Edition* (Cambridge University Press, 2010).

[34] G. M. D'Ariano, M. G. Paris, and M. F. Sacchi, *Advances in imaging and electron physics* **128**, 206 (2003).

[35] R. Yang and Y. Li, *Physical Review A* **103**, 032421 (2021).

[36] B. Wu, M. Ray, L. Zhao, X. Sun, and P. Rebentrost, *Physical Review A* **103**, 042422 (2021).

[37] L. Xu, X.-Y. Zhang, J.-M. Liang, J. Wang, M. Li, L. Jian, and S.-q. Shen, *Communications in Theoretical Physics* **74**, 055106 (2022).

[38] T. L. Patti, J. Kossaifi, A. Anandkumar, and S. F. Yelin, *Quantum* **7**, 1057 (2023).

[39] D. Aharonov, V. Jones, and Z. Landau, in *Proceedings of the thirty-eighth annual ACM symposium on Theory of computing* (2006) pp. 427–436.

[40] D. Greenbaum, arXiv preprint arXiv:1509.02921 (2015).

[41] G. Torlai, G. Mazzola, J. Carrasquilla, M. Troyer, R. Melko, and G. Carleo, *Nature Physics* **14**, 447 (2018).

[42] M. Cramer, M. B. Plenio, S. T. Flammia, R. Somma, D. Gross, S. D. Bartlett, O. Landon-Cardinal, D. Poulin, and Y.-K. Liu, *Nature communications* **1**, 149 (2010).

[43] M. Mohseni, A. T. Rezakhani, and D. A. Lidar, *Physical Review A* **77**, 032322 (2008).

[44] J. B. Altepeter, D. Branning, E. Jeffrey, T. Wei, P. G. Kwiat, R. T. Thew, J. L. O'Brien, M. A. Nielsen, and A. G. White, *Physical Review Letters* **90**, 193601 (2003).

[45] R. Blume-Kohout, J. K. Gamble, E. Nielsen, J. Mizrahi, J. D. Sterk, and P. Maunz, arXiv preprint arXiv:1310.4492 (2013).

[46] M. G. Cowling and J. F. Price, *SIAM journal on mathematical analysis* **15**, 151 (1984).

## Appendix A: Completeness Proof

In the main text, the calculation of  $Tr\{\rho^k\}$  has been mathematically transformed into investigating  $Tr\{G^k\}$ , where  $Tr\{G^k\}$  represents the trace of  $G^k$ , which is obtained by decomposing the mixed state into pure states and then

taking a weighted average. Therefore, the primary focus is on calculating  $Tr\{\mathcal{G}_q^k\}$ .

After selecting a combination  $\mathcal{G}_q^k : G_{q_1}G_{q_2} \cdots G_{q_t} \cdots G_{q_k}$ , it is necessary to determine the dimension of the subspace  $d$ . For the subspace determined by the combination  $\mathcal{G}_q^k$ , if the dimension of the subspace is  $d$ , then the quantum states  $\rho_s$  prepared by different random gates of dimension  $d$ , where  $s \in \{1, 2, \dots, d\}$ , are guaranteed to be linearly independent. Preparation of  $d$  linearly independent quantum states using  $d$   $n$ -bit random gates:  $\rho_s = U_s|0\rangle\langle 0|^{\otimes n}U_s^\dagger$ . The random gate  $U_s$  belongs to different random gates within a certain combination  $\mathcal{G}_q^k$ .

Preparation of the remaining  $d^2 - d$  quantum states: Assuming we have already prepared  $d$  linearly independent quantum states:  $\rho_1, \rho_2, \dots, \rho_d$ , we need to prepare an additional  $d^2 - d$  quantum states to form a complete  $d^2$ -dimensional inner product space. In a finite-dimensional linear space, it is sufficient for all  $d^2$  quantum states to be linearly independent from each other.

For the quantum state  $\rho_s = U_s|0\rangle\langle 0|^{\otimes n}U_s^\dagger$ , where  $s, s' \in \{1, 2, \dots, d\}, s \neq s'$ , we apply the quantum gate  $G_{s'} = U_{s'}G_0U_{s'}^\dagger = I - 2\rho_{s'}$  to obtain:

$$\begin{aligned} \rho_{ss'} &= G_{s'}\rho_sG_{s'}^\dagger = (I - 2\rho_{s'})\rho_s(I - 2\rho_{s'}) \\ &= \rho_s - 2\rho_{s'}\rho_s - 2\rho_s\rho_{s'} + 4\rho_{s'}\rho_s\rho_{s'}. \end{aligned} \quad (\text{A1})$$

For the corresponding  $\rho_{s's}$ , we have:

$$\rho_{s's} = \rho_{s'} - 2\rho_{s'}\rho_s - 2\rho_s\rho_{s'} + 4\rho_s\rho_{s'}\rho_s. \quad (\text{A2})$$

It can be shown that the quantum states  $\rho_s, \rho_{s'}, \rho_{ss'}, \rho_{s's}$  are linearly dependent. If we construct all quantum states using this method, then these quantum states will be linearly dependent and cannot form a complete  $d^2$ -dimensional inner product space.

To ensure linear independence, we modify the gate  $G_0$  to  $G_\theta$ , where  $\theta \neq k\pi, k \in \mathbb{Z}$ :

$$G_0 = \begin{pmatrix} -1 & 0 & \cdots & 0 \\ 0 & 1 & \cdots & 0 \\ \vdots & \vdots & \ddots & \vdots \\ 0 & 0 & \cdots & 1 \end{pmatrix} \longrightarrow G_\theta = \begin{pmatrix} e^{i\theta} & 0 & \cdots & 0 \\ 0 & 1 & \cdots & 0 \\ \vdots & \vdots & \ddots & \vdots \\ 0 & 0 & \cdots & 1 \end{pmatrix} = \begin{pmatrix} 1 & 0 & \cdots & 0 \\ 0 & 1 & \cdots & 0 \\ \vdots & \vdots & \ddots & \vdots \\ 0 & 0 & \cdots & 1 \end{pmatrix} - \begin{pmatrix} 1 - e^{i\theta} & 0 & \cdots & 0 \\ 0 & 1 & \cdots & 0 \\ \vdots & \vdots & \ddots & \vdots \\ 0 & 0 & \cdots & 1 \end{pmatrix} \quad (\text{A3})$$

After this change, the transformed  $G_s(\theta) = U_sG_\theta U_s^\dagger$ . We represent  $G_s(\theta) = U_sG(\theta)U_s^\dagger$  as  $G_s(\theta) = I - \rho_s(\theta)$ , and  $\rho_s(\theta) \neq \rho_s$ . Following the same approach as before, we prepare the quantum states:

$$\begin{aligned} 1. \rho_s &= U_s|0\rangle\langle 0|^{\otimes n}U_s^\dagger, \\ 2. \rho_{s'} &= U_{s'}|0\rangle\langle 0|^{\otimes n}U_{s'}^\dagger, \\ 3. \rho_{ss'} &= (I - 2\rho_{s'})\rho_s(I - 2\rho_{s'}) \\ &= \rho_s - 2\rho_{s'}\rho_s - 2\rho_s\rho_{s'} + 4\rho_{s'}\rho_s\rho_{s'}, \\ 4. \rho_{s's}(\theta) &= G_s(\theta)\rho_{s'}G_s(\theta)^\dagger \\ &= (I - \rho_s(\theta))\rho_{s'}(I - \rho_s(\theta)) \\ &= \rho_{s'} - \rho_{s'}\rho_s(\theta) - \rho_s(\theta)\rho_{s'} + \rho_s(\theta)\rho_{s'}\rho_s(\theta). \end{aligned} \quad (\text{A4})$$

From the above equation, we observe that rotating the quantum gate  $G_0$  by an arbitrary angle  $\theta \neq k\pi, k = 0, 1, 2, \dots$  changes the originally linearly dependent quantum states, prepared using  $G_0$ , into linearly independent ones.

By using similar methods, it is possible to prepare the remaining  $d(d - 1)$  quantum states and ensure that they are linearly independent. This allows us to construct a complete  $d^2$ -dimensional linear space for performing a full tomography of the PTM (Process Tensor Matrix) under study.

## Appendix B: More Numerical Simulation

For the Hadamard Test procedure, we incorporate noise simulation into its measurement process by injecting random numbers drawn from a Gaussian distribution with a standard deviation of 0.01. The graphical representation below illustrates the outcomes prior to and subsequent to the integration of these random numbers:

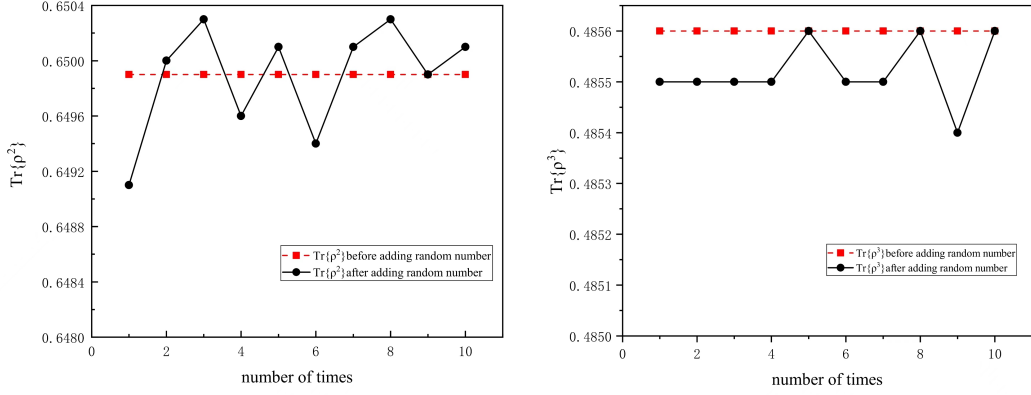


FIG. 4. The values of  $Tr\{\rho^2\}$  and  $Tr\{\rho^3\}$  calculated using the Hadamard Test, with the black line representing the results after adding random numbers, and the red line representing the results before adding random gates.

For Tomography, we introduce noise simulation by adding random numbers to its PTM (Pauli Transfer Matrix) elements as well as g-matrix elements. Since the singular values of the g-matrix are small, we choose random numbers sampled from a Gaussian distribution with a standard deviation of 0.0001 to simulate the noise. The results before and after adding the random numbers are shown in the graph below:

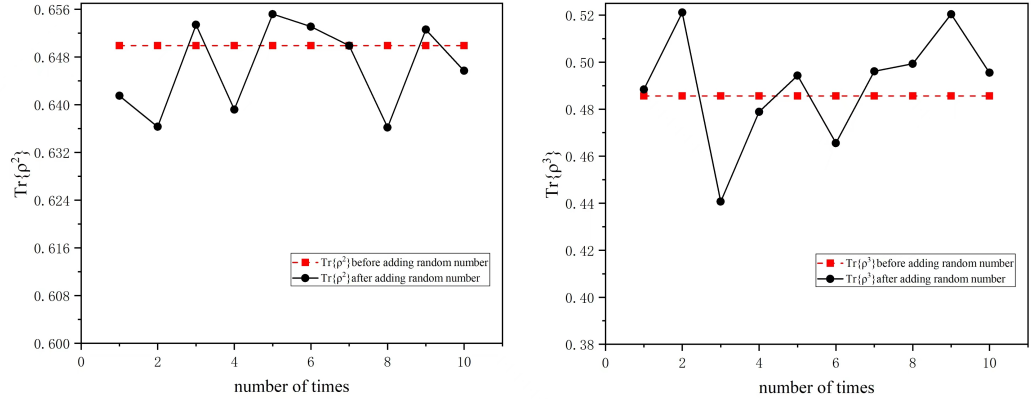


FIG. 5. The values of  $Tr\{\rho^2\}$  and  $Tr\{\rho^3\}$  calculated using Tomography, with the black line representing the results after adding random numbers, and the red line representing the results before adding random gates.

Derived from the data depicted in the provided graph, we are able to distinctly discern the repercussions stemming from the introduction or absence of noise. When noise is absent, the output data from the quantum circuit manifests as consistently stable and precise. Nonetheless, the scenario takes a discernible turn upon the infusion of noise. The introduction of noise precipitates volatility in the quantum circuit's outcomes, potentially culminating in errors. Noise can engender an unreliable exchange of information amidst quantum bits, thereby injecting substantial ambiguity into the computational process. These sources of noise might encompass phenomena such as dephasing, errors in quantum gate operations, imprecisions in measurements, or other external disturbances.

In real-world scenarios, noise presents a significant hurdle for the advancement of quantum computing and quantum information processing. To counteract the disruptive influence of noise, researchers are tirelessly engaged in refining

quantum error correction and noise suppression techniques. The primary goal of these approaches is to bolster the resilience of quantum circuits and heighten the precision of outcomes, ultimately striving for a more dependable realm of quantum computing. Furthermore, the ramifications of noise can exhibit variability across diverse quantum algorithms and tasks. As a result, practical applications necessitate a thorough assessment of algorithm robustness alongside the prevailing noise levels. Achieving equilibrium between these considerations is crucial in determining the most optimal course of action.

### Appendix C: Subspace dimension

In this article, we study the dimensions of the invariant subspaces corresponding to nonlinear functions of different types of density matrices. Let's start with the simplest case,  $Tr\{\rho^m\}$ . In our algorithm, we decompose the computation of  $Tr\{\rho^m\}$  into the computation of  $Tr\{G_{q_1}G_{q_2}\dots G_{q_k}\}$ , for  $k = 0, 1, \dots, m$ . It is obvious that  $span(|\psi_{q_1}\rangle, |\psi_{q_2}\rangle, \dots, |\psi_{q_k}\rangle)$  forms a non-trivial invariant subspace of  $G_{q_1}G_{q_2}\dots G_{q_k}$ . Therefore, the largest non-trivial invariant subspace involved in the calculation of  $Tr\{\rho^m\}$  is  $m$ -dimensional.

A more general nonlinear function is  $Tr\{P_1\rho_1P_2\rho_2\dots P_m\rho_m\}$ . We can rewrite this function as  $Tr\{P'\rho'_1\rho'_2\dots \rho'_m\}$ , where  $\rho'_i = (\Pi_{l=1}^i P_l)\rho_n(\Pi_{l=1}^i P_l)^\dagger$  and  $P' = \Pi_{l=1}^i P_l$ . Remark that although  $\rho'_1 \neq \rho'_2 \neq \dots \neq \rho'_m$ , the algorithms we proposed in this paper can also be used. During the calculation, we need to calculate  $Tr\{P'G_{q_1}G_{q_2}\dots G_{q_k}\}$ , for  $k = 0, 1, \dots, m$ , where  $P'$  is a Pauli operator. Note that  $G_{q_i}$  acts on  $|\psi\rangle$  to get a superposition of  $|\psi_{q_i}\rangle$  and  $|\psi\rangle$ . Thus the non-trivial invariant subspace corresponding to  $P G_{q_1}G_{q_2}\dots G_{q_k}$  is  $span(|\psi_{q_1}\rangle, \dots, |\psi_{q_m}\rangle, P|\psi_{q_1}\rangle, \dots, P|\psi_{q_m}\rangle)$ , of which the largest possible dimension is  $2m$  dimensions.